applied optics

Progressive algorithm for the scattering of electromagnetic waves by a multilayered eccentric sphere

Rongheng Li and Ben Q. Li*

Department of Mechanical Engineering, University of Michigan, Dearborn, Michigan 48128, USA
**benqli@umich.edu*

Received 13 April 2023; revised 4 June 2023; accepted 6 June 2023; posted 6 June 2023; published 10 July 2023

This paper presents a general progressive algorithm for the computational study of electromagnetic wave scattering by a multilayered eccentric nanoparticle. The presented methodology is based on a combination of the vector addition theorem for spherical wave functions and an efficient progressive algorithm that matches the boundary conditions of every two adjacent shell layers from the outmost to the innermost layer. As a result, only a solution of small-sized matrices is required rather than solving a large set of system equations as reported in other works. With the developed approach, explicit expressions of the Mie scattering coefficients of the eccentric particle can be obtained. Moreover, the Mie coefficients of a specific inner layer could be calculated selectively, instead of having to compute those of all layers of the entire particle as required by other algorithms. The presented methodology can be used to study practically any type of spherical particle inclusions and the most widely studied cases such as scattering by solid particles, concentric particles, and inclusions with centers displaced along a straight line are just special cases of the algorithm presented. Computed results are also presented, illustrating that the eccentric structure allows extra freedom in the design of multilayered nanoparticles for optical applications.

https://doi.org/10.1364/AO.493117

1. INTRODUCTION

Nanoparticles made of metals and high refractive index dielectrics are attractive in the optical domain due to their strong resonance scattering and absorption responses. Such excellent optical properties are flavored in various applications, including photovoltaics [1–3], solar water splitting [4–6], biosensing [7–9], solar collector [10–12], and solar desalination [13–15]. In the design aspect, the optical response of a spherical nanoparticle is characterized by its material composition and radius [16]. Distinct material composition selections provide different mode resonances, whereas, the radius is usually utilized to shift the peak of resonances. For a solid nanoparticle, such tunability is limited due to its simple structure. Multilayered spherical structure drastically extends the freedom of adjusting the resonances since it contains more material species. The tunability of distinct mode resonance peaks enables single particles to achieve unique optical features, i.e., forward scattering, transverse scattering, and strong absorption. Liu *et al.* presented core/shell nanoparticles that scatter the light in the forward direction [17]. The resonance peaks of electric and magnetic modes are engineered by changing the radii and material compositions of the shell layers. Shamkhi *et al.* demonstrated a novel transverse scattering effect where both forward and backward scattered fields are suppressed [18]. Such an effect is achieved through the interference between the electric dipole and the off-resonant quadrupole. Gong *et al.* reported a three-layered $Ag-SiO_2-Ag$ nanoparticle that boosts solar absorption 2.28 times compared to the solid silver particle with the same dimensions [19]. Several absorption peaks are obtained with the core/shell structure fine-tuned. Yang and co-workers presented nanostructures containing distinct nanoparticles, i.e., silicon particles, a gold nanosphere, and a gold nanorod, to enhance the light emission of quantum dots [20–23]. The resonance peak of nanoparticles may be tuned to the same frequency as the photoluminescence of quantum dots. Furthermore, particles with eccentric core/shell structures provide extra tunability, which yields better optical responses. Yang *et al.* presented a depth-varying silicon crescent shell array, i.e., a two-layered eccentric core/shell structure, that possesses broadband light absorption [24]. An optimal light trapping capacity may be obtained by tuning the radii of shell layers and the depth that the core is embedded in the outer layer.

These particle structure designs are based on the theory to compute the optical responses of multilayered particles. The Mie theory provides the analytical solution to the scattering problem where an electromagnetic plane wave strikes a homogeneous, linear, and nonmagnetic sphere [25]. It is generalized to study the responses of coated shells [26], multilayered spheres [27–29], multilayered spheroidal particles [30], a nanoparticle

aggregate [31–37], and gyrotropic spherical particles [38,39]. In practical implementation, matching the boundary conditions between adjacent layers often yields a large system of linear equations. Solving them simultaneously results in a complex calculation load, especially for particles containing many shell layers. For instance, Liu designed a core/shell spherical structure that contains more than 50 shell layers to achieve radial anisotropy [40], which yields an intensive computational task. Instead of directly inverse the linear system, Yang presented a recursive algorithm, which calculates the Mie scattering coefficients by sweeping back and forth through the entire particle between the outmost and the innermost layers [41]. Peña and Pal implemented the recursive algorithm in a computer program [42]. Coupled with the addition theorem [43,44], it is further extended to calculate the scattering coefficients of multilayered particle aggregates [45]. Moroz introduced a transfer-matrix approach for a multilayered concentric spherical particle [46], which matches the boundary conditions between adjacent shell layers by employing transfer matrices. Our previous work presents an efficient progressive algorithm that implements the boundary conditions from the innermost to the outmost layer with only matrix multiplication required [47]. It is applicable for an eccentric paticle with all the inner cores displaced along in the same direction. Moreover, the progressive algorithem may be simplified to study the scattering characteristics of a concentric core/shell particle. However, an algorithm that is suitable for more general eccentric core/shell structures where the centers of the inner shells do not form a line of axisymmetry has not been developed yet.

In this paper, a general progressive algorithm is presented for the computational study of the scattering of electromagnetic waves by a multilayered eccentric nanoparticle. The boundary conditions between every two adjacent layers are progressively implemented from the outmost to the innermost layer with small matrix multiplications needed. In matching the boundary conditions at the interface of adjacent layers, the vector addition theorem is applied. The expressions of the scattering coefficients of the entire particles are obtained. In addition, the Mie coefficients of any specific shell layer may be computed directly rather than having to calculate those of other layers at the same time. In the following sections, we present the mathematical derivation and formulation of the progressive algorithm for a multilayered eccentric core/shell particle. With this algorithm, a concentric multilayered particle, which has been studied extensively in the literature, is just a special case of this general algorithm. Numerical cases show that the proposed approach can be utilized in the design of core/shell particles with distinct scattering characteristics. It is worth noting that the progressive algorithm is applicable for particles with any size parameters, not only being limited to nanosized particles.

2. MATHEMATICAL ANALYSIS

A multilayered eccentric shell configuration is displayed in Fig. 1. The electromagnetic wave incidents along the $\mathbf{k}$ direction where the time dependence is assumed as $e^{-i\omega t}$. The incident radiation forms an angle α with the z coordinate, and the electric field is linearly polarized in the direction of $\mathbf{e}_E = -\cos\alpha\cos\gamma\mathbf{e}_x + \sin\gamma\mathbf{e}_y + \sin\alpha\cos\gamma\mathbf{e}_z$, where γ is the angle of the electric field with a line in the plane perpendicular to the propagation direction. For convenience, the center of the largest sphere is at the origin of the global coordinate system. Note that the centers of the shells in the structure under consideration do not form a line of axisymmetry.

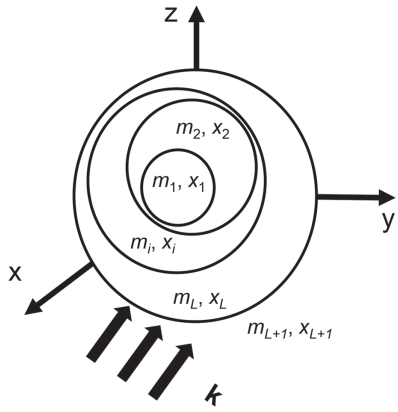

Fig. 1. Configuration of a single multilayered eccentric particle.

The physics of fields outside and inside the multilayered eccentric shell is governed by the Maxwell equations, which for the problem under consideration, reduce to the vector wave equations,

$$\nabla^2\mathbf{E} + k^2\mathbf{E} = \mathbf{0}, \quad \nabla\cdot\mathbf{E} = 0, \quad \mathbf{H} = -(i/\omega)\nabla\times\mathbf{E}, \quad k^2 = \omega m/c, \tag{1}$$

where $\mathbf{E}$ and $\mathbf{H}$ are the electric and magnetic fields. m and c are the refractive index and the speed of light, respectively. The field expansion and the vector addition theorem are involved in the process of achieving the analytical solution of the above equations.

To begin with, the solution of the wave equations for any two adjacent layers l and $l+1$ may be expanded as

$$\mathbf{E}_l = \sum_{n=1}^{\infty}\sum_{m=-n}^{n} E_n\left(c_{mn}^l\mathbf{M}_{mn,l}^{(1)} + d_{mn}^l\mathbf{N}_{mn,l}^{(1)} + b_{mn}^l\mathbf{M}_{mn,l}^{(3)} + a_{mn}^l\mathbf{N}_{mn,l}^{(3)}\right), \tag{2}$$

$$\mathbf{H}_l = -\frac{im_l}{\omega\mu}\sum_{n=1}^{\infty}\sum_{m=-n}^{n} E_n \times\left(d_{mn}^l\mathbf{M}_{mn,l}^{(1)} + c_{mn}^l\mathbf{N}_{mn,l}^{(1)} + a_{mn}^l\mathbf{M}_{mn,l}^{(3)} + b_{mn}^l\mathbf{N}_{mn,l}^{(3)}\right), \tag{3}$$

$$\mathbf{E}_{l+1} = \sum_{n=1}^{\infty}\sum_{m=-n}^{n} E_n\left(c_{mn}^{l+1}\mathbf{M}_{mn,l+1}^{(1)} + d_{mn}^{l+1}\mathbf{N}_{mn,l+1}^{(1)} + b_{mn}^{l+1}\mathbf{M}_{mn,l+1}^{(3)} + a_{mn}^{l+1}\mathbf{N}_{mn,l+1}^{(3)}\right), \tag{4}$$

$$\mathbf{H}_{l+1} = -\frac{im_{l+1}}{\omega\mu}\sum_{n=1}^{\infty}\sum_{m=-n}^{n} E_n\left(d_{mn}^{l+1}\mathbf{M}_{mn,l+1}^{(1)} + c_{mn}^{l+1}\mathbf{N}_{mn,l+1}^{(1)} + a_{mn}^{l+1}\mathbf{M}_{mn,l+1}^{(3)} + b_{mn}^{l+1}\mathbf{N}_{mn,l+1}^{(3)}\right), \tag{5}$$

with a_{mn}, b_{mn}, c_{mn}, and d_{mn} as the expansion coefficients. Note that $E_n = i^n E_0(2n+1)/n(n+1)$ for a plane wave with E_0 as the magnitude of the electric field [33]. Superscripts l and $l+1$ denote two adjacent layers of the multilayered eccentric shell, respectively. The vector wave-functions $\mathbf{M}_{mn}$ and $\mathbf{N}_{mn}$ are expressed as [43,44]

$$\mathbf{M}_{mn}^{(q)} = \frac{im}{\sin\theta} z_n^{(q)}(kr) P_n^m(\cos\theta) e^{im\varphi}\mathbf{e}_\theta - z_n^{(q)}(kr)\frac{\partial P_n^m(\cos\theta)}{\partial\theta} e^{im\varphi}\mathbf{e}_\varphi, \tag{6}$$

$$\begin{aligned}\mathbf{N}_{mn}^{(q)} = {} & \frac{1}{kr} z_n^{(q)}(kr) n(n+1) P_n^m(\cos\theta) e^{im\varphi}\mathbf{e}_r \\ & + \frac{1}{kr}\frac{\partial\left[r z_n^{(q)}(kr)\right]}{\partial r}\frac{\partial P_n^m(\cos\theta)}{\partial\theta} e^{im\varphi}\mathbf{e}_\theta \\ & + \frac{im}{kr\sin\theta}\frac{\partial\left[r z_n^{(q)}(kr)\right]}{\partial r} P_n^m(\cos\theta) e^{im\varphi}\mathbf{e}_\varphi,\end{aligned} \tag{7}$$

where $P_n^m(\cos\theta)$ are the associated Legendre polynomials. $z_n^{(q)}$ is the spherical Bessel function of the first kind $j_n(kr)$, and the spherical Hankel function of the first kind $h_n^1(kr)$ with q is denoted as 1 and 2, respectively.

To satisfy the boundary conditions along the particle interface, $\mathbf{M}_{mn}$ and $\mathbf{N}_{mn}$ functions need to be transferred to the same coordinate by utilizing the vector addition theorem. The detailed derivation of addition theorems and the expressions of the translation coefficients may be found in works already published [43,44,48], and, thus, only the final results are given below for the vector functions in the $(l+1)$th layer in terms of those in the lth layer,

$$\mathbf{M}_{mn,l+1}^{(1)} = \sum_{\nu=1}^{\infty}\sum_{\mu=-\nu}^{\nu}\left(A_{mn,l}^{\mu\nu}\mathbf{M}_{\mu\nu,l,l+1}^{(1)} + B_{mn,l}^{\mu\nu}\mathbf{N}_{\mu\nu,l,l+1}^{(1)}\right), \tag{8}$$

$$\mathbf{N}_{mn,l+1}^{(1)} = \sum_{\nu=1}^{\infty}\sum_{\mu=-\nu}^{\nu}\left(B_{mn,l}^{\mu\nu}\mathbf{M}_{\mu\nu,l,l+1}^{(1)} + A_{mn,l}^{\mu\nu}\mathbf{N}_{\mu\nu,l,l+1}^{(1)}\right), \tag{9}$$

$$\mathbf{M}_{mn,l+1}^{(3)} = \sum_{\nu=1}^{\infty}\sum_{\mu=-\nu}^{\nu}\left(A_{mn,l}^{\mu\nu}\mathbf{M}_{\mu\nu,l,l+1}^{(3)} + B_{mn,l}^{\mu\nu}\mathbf{N}_{\mu\nu,l,l+1}^{(3)}\right), \tag{10}$$

$$\mathbf{N}_{mn,l+1}^{(3)} = \sum_{\nu=1}^{\infty}\sum_{\mu=-\nu}^{\nu}\left(B_{mn,l}^{\mu\nu}\mathbf{M}_{\mu\nu,l,l+1}^{(3)} + A_{mn,l}^{\mu\nu}\mathbf{N}_{\mu\nu,l,l+1}^{(3)}\right), \tag{11}$$

where the subscripts l, $l+1$ means that the coordinates of the $(l+1)$th shell are translated at the lth layer. $A_{nm,l}^{\nu\mu}$ and $B_{nm,l}^{\nu\mu}$ are the translational coefficients of the addition theorem [43–45].

With the above substituted into Eqs. (4) and (5) followed by interchanging index $(m \leftrightarrow \mu,\ n \leftrightarrow \nu)$, we have

$$\begin{aligned}\mathbf{E}_{l+1} = {} & \sum_{n=1}^{\infty}\sum_{m=-n}^{n}\left(q_{mn}^{l+1}\mathbf{M}_{mn,l,l+1}^{(1)} + r_{mn}^{l+1}\mathbf{N}_{mn,l,l+1}^{(1)}\right. \\ & \left. + s_{mn}^{l+1}\mathbf{M}_{mn,l,l+1}^{(3)} + t_{mn}^{l+1}\mathbf{N}_{mn,l,l+1}^{(3)}\right),\end{aligned} \tag{12}$$

and similarly,

$$\begin{aligned}\mathbf{H}_{l+1} = {} & -\frac{im_{l+1}}{\omega\mu}\sum_{n=1}^{\infty}\sum_{m=-n}^{n}\left(r_{mn}^{l+1}\mathbf{M}_{mn,l,l+1}^{(1)} + q_{mn}^{l+1}\mathbf{N}_{mn,l,l+1}^{(1)}\right. \\ & \left. + t_{mn}^{l+1}\mathbf{M}_{mn,l,l+1}^{(3)} + s_{mn}^{l+1}\mathbf{N}_{mn,l,l+1}^{(3)}\right),\end{aligned} \tag{13}$$

where

$$q_{mn}^{l+1} = \sum_{\nu=1}^{\infty}\sum_{\mu=-\nu}^{\nu}\left(c_{\mu\nu}^{l+1}A_{\mu\nu,l}^{mn} + d_{\mu\nu}^{l+1}B_{\mu\nu,l}^{mn}\right), \tag{14}$$

$$r_{mn}^{l+1} = \sum_{\nu=1}^{\infty}\sum_{\mu=-\nu}^{\nu}\left(c_{\mu\nu}^{l+1}B_{\mu\nu,l}^{mn} + d_{\mu\nu}^{l+1}A_{\mu\nu,l}^{mn}\right), \tag{15}$$

$$s_{mn}^{l+1} = \sum_{\nu=1}^{\infty}\sum_{\mu=-\nu}^{\nu}\left(b_{\mu\nu}^{l+1}A_{\mu\nu,l}^{mn} + a_{\mu\nu}^{l+1}B_{\mu\nu,l}^{mn}\right), \tag{16}$$

$$t_{mn}^{l+1} = \sum_{\nu=1}^{\infty}\sum_{\mu=-\nu}^{\nu}\left(b_{\mu\nu}^{l+1}B_{\mu\nu,l}^{mn} + a_{\mu\nu}^{l+1}A_{\mu\nu,l}^{mn}\right). \tag{17}$$

In practical calculations, a terminal value N needs to be set on ν, and N is chosen to satisfy the required accuracy. Rearrange the summation order of indices m, n, μ, and ν,

$$\begin{aligned}\mathbf{E}_{l+1} = {} & \sum_{m=-N}^{N}\sum_{n=|m|}^{N}\left(q_{mn}^{l+1}\mathbf{M}_{mn,l,l+1}^{(1)} + r_{mn}^{l+1}\mathbf{N}_{mn,l,l+1}^{(1)}\right. \\ & \left. + s_{mn}^{l+1}\mathbf{M}_{mn,l,l+1}^{(3)} + t_{mn}^{l+1}\mathbf{N}_{mn,l,l+1}^{(3)}\right),\end{aligned} \tag{18}$$

$$\begin{aligned}\mathbf{H}_{l+1} = {} & -\frac{im_{l+1}}{\omega\mu}\sum_{m=-N}^{N}\sum_{n=|m|}^{N}\left(r_{mn}^{l+1}\mathbf{M}_{mn,l,l+1}^{(1)} + q_{mn}^{l+1}\mathbf{N}_{mn,l,l+1}^{(1)}\right. \\ & \left. + t_{mn}^{l+1}\mathbf{M}_{mn,l,l+1}^{(3)} + s_{mn}^{l+1}\mathbf{N}_{mn,l,l+1}^{(3)}\right).\end{aligned} \tag{19}$$

For the discussions to follow, it is more convenient to write those coefficients in matrix form,

$$\{qt\}^{l+1} = \begin{bmatrix} t_{-N,N}^{l+1} \\ s_{-N,N}^{l+1} \\ q_{-N,N}^{l+1} \\ r_{-N,N}^{l+1} \\ \vdots \\ t_{mn}^{l+1} \\ s_{mn}^{l+1} \\ q_{mn}^{l+1} \\ r_{mn}^{l+1} \\ \vdots \end{bmatrix} = [\mathrm{S}]_l \begin{bmatrix} a_{-N,N}^{l+1} \\ b_{-N,N}^{l+1} \\ c_{-N,N}^{l+1} \\ d_{-N,N}^{l+1} \\ \vdots \\ a_{mn}^{l+1} \\ b_{mn}^{l+1} \\ c_{mn}^{l+1} \\ d_{mn}^{l+1} \\ \vdots \end{bmatrix} = [\mathrm{S}]_l\{ad\}^{l+1}, \tag{20}$$

with index n going from 1 to N, whereas, m from $-n$ to n. Specifically, $\{qt\}^{l+1}$ and $\{ad\}^{l+1}$ are vectors of $4N(N+2)$ dimensions. Also, $[\mathrm{S}]_l$ is a matrix of $4N(N+2)\times 4N(N+2)$ dimensions containing the translation coefficients $A_{\mu\nu,l}^{mn}$ and $B_{\mu\nu,l}^{mn}$,

$$[\mathrm{S}]_l = \begin{bmatrix} [\mathrm{S}]^{-N,N}_{-N,N,l} & [\mathrm{S}]^{-N,N}_{-(N-1),N-1,l} & [\mathrm{S}]^{-N,N}_{-(N-1),N,l} & \cdots & [\mathrm{S}]^{-N,N}_{\mu\nu,l} & \cdots & [\mathrm{S}]^{-N,N}_{NN,l} \\ [\mathrm{S}]^{-(N-1),N-1}_{-N,N,l} & [\mathrm{S}]^{-(N-1),N-1}_{-(N-1),N-1,l} & [\mathrm{S}]^{-(N-1),N-1}_{-(N-1),N,l} & \cdots & [\mathrm{S}]^{-(N-1),N-1}_{\mu\nu,l} & \cdots & [\mathrm{S}]^{-(N-1),N-1}_{NN,l} \\ [\mathrm{S}]^{-(N-1),N}_{-N,N,l} & [\mathrm{S}]^{-(N-1),N}_{-(N-1),N-1,l} & [\mathrm{S}]^{-(N-1),N}_{-(N-1),N,l} & \cdots & [\mathrm{S}]^{-(N-1),N}_{\mu\nu,l} & \cdots & [\mathrm{S}]^{-(N-1),N}_{NN,l} \\ \vdots & \vdots & \vdots & \ddots & \vdots & & \vdots \\ [\mathrm{S}]^{mn}_{-N,N,l} & [\mathrm{S}]^{mn}_{-(N-1),N-1,l} & [\mathrm{S}]^{mn}_{-(N-1),N,l} & \cdots & [\mathrm{S}]^{mn}_{\mu\nu,l} & \cdots & [\mathrm{S}]^{mn}_{NN,l} \\ \vdots & \vdots & \vdots & & \vdots & \ddots & \vdots \\ [\mathrm{S}]^{NN}_{-N,N,l} & [\mathrm{S}]^{NN}_{-(N-1),N-1,l} & [\mathrm{S}]^{NN}_{-(N-1),N,l} & \cdots & [\mathrm{S}]^{NN}_{\mu\nu,l} & \cdots & [\mathrm{S}]^{NN}_{NN,l} \end{bmatrix}, \tag{21}$$

$$[\mathrm{S}]^{mn}_{\mu\nu,l} = \begin{bmatrix} A^{mn}_{\mu\nu,l} & 0 & B^{mn}_{\mu\nu,l} & 0 \\ 0 & A^{mn}_{\mu\nu,l} & 0 & B^{mn}_{\mu\nu,l} \\ B^{mn}_{\mu\nu,l} & 0 & A^{mn}_{\mu\nu,l} & 0 \\ 0 & B^{mn}_{\mu\nu,l} & 0 & A^{mn}_{\mu\nu,l} \end{bmatrix} = \begin{bmatrix} A^{mn}_{\mu\nu,l}[\mathrm{I}] & B^{mn}_{\mu\nu,l}[\mathrm{I}] \\ B^{mn}_{\mu\nu,l}[\mathrm{I}] & A^{mn}_{\mu\nu,l}[\mathrm{I}] \end{bmatrix}. \tag{22}$$

The electric and magnetic fields in Eqs. (2) and (5), after the vector translation described by Eqs. (8)–(11), are all defined in the same coordinate system, that is, the spherical coordinate system associated with the lth layer. These fields are made to satisfy the continuity conditions on the tangential electric and magnetic fields along the interface between layers l and $l+1$,

$$(\mathbf{E}_{l+1} - \mathbf{E}_l) \times e_r = \mathbf{0}, \tag{23}$$

$$(\mathbf{H}_{l+1} - \mathbf{H}_l) \times e_r = \mathbf{0}. \tag{24}$$

Substituting Eqs. (2)–(5) and (18)–(20) into Eqs. (23) and (24) results in a linear system,

$$\{ad\}^l = [\mathrm{Q}]_l \{ad\}^{l+1}, \tag{25}$$

with

$$[\mathrm{Q}]_l = \begin{bmatrix} [\mathrm{Q}]^{-N,N}_{-N,N,l} & [\mathrm{Q}]^{-N,N}_{-(N-1),N-1,l} & [\mathrm{Q}]^{-N,N}_{-(N-1),N,l} & \cdots & [\mathrm{Q}]^{-N,N}_{\mu\nu,l} & \cdots & [\mathrm{Q}]^{-N,N}_{NN,l} \\ [\mathrm{Q}]^{-(N-1),N-1}_{-N,N,l} & [\mathrm{Q}]^{-(N-1),N-1}_{-(N-1),N-1,l} & [\mathrm{Q}]^{-(N-1),N-1}_{-(N-1),N,l} & \cdots & [\mathrm{Q}]^{-(N-1),N-1}_{\mu\nu,l} & \cdots & [\mathrm{Q}]^{-(N-1),N-1}_{NN,l} \\ [\mathrm{Q}]^{-(N-1),N}_{-N,N,l} & [\mathrm{Q}]^{-(N-1),N}_{-(N-1),N-1,l} & [\mathrm{Q}]^{-(N-1),N}_{-(N-1),N,l} & \cdots & [\mathrm{Q}]^{-(N-1),N}_{\mu\nu,l} & \cdots & [\mathrm{Q}]^{-(N-1),N}_{NN,l} \\ \vdots & \vdots & \vdots & \ddots & \vdots & & \vdots \\ [\mathrm{Q}]^{mn}_{-N,N,l} & [\mathrm{Q}]^{mn}_{-(N-1),N-1,l} & [\mathrm{Q}]^{mn}_{-(N-1),N,l} & \cdots & [\mathrm{Q}]^{mn}_{\mu\nu,l} & \cdots & [\mathrm{Q}]^{mn}_{NN,l} \\ \vdots & \vdots & \vdots & & \vdots & \ddots & \vdots \\ [\mathrm{Q}]^{NN}_{-N,N,l} & [\mathrm{Q}]^{NN}_{-(N-1),N-1,l} & [\mathrm{Q}]^{NN}_{-(N-1),N,l} & \cdots & [\mathrm{Q}]^{NN}_{\mu\nu,l} & \cdots & [\mathrm{Q}]^{NN}_{NN,l} \end{bmatrix}, \tag{26}$$

$$[\mathrm{Q}]^{mn}_{\mu\nu,l} = \begin{bmatrix} q^{mn}_{\mu\nu,l,11} & q^{mn}_{\mu\nu,l,12} & q^{mn}_{\mu\nu,l,13} & q^{mn}_{\mu\nu,l,14} \\ q^{mn}_{\mu\nu,l,21} & q^{mn}_{\mu\nu,l,22} & q^{mn}_{\mu\nu,l,23} & q^{mn}_{\mu\nu,l,24} \\ q^{mn}_{\mu\nu,l,31} & q^{mn}_{\mu\nu,l,32} & q^{mn}_{\mu\nu,l,33} & q^{mn}_{\mu\nu,l,34} \\ q^{mn}_{\mu\nu,l,41} & q^{mn}_{\mu\nu,l,42} & q^{mn}_{\mu\nu,l,43} & q^{mn}_{\mu\nu,l,44} \end{bmatrix}, \tag{27}$$

$$q^{mn}_{\mu\nu,l,11} = A^{mn}_{\mu\nu,l} \frac{m_{l+1}\xi_n(m_{l+1}x_l)\psi_n'(m_lx_l) - m_l\xi_n'(m_{l+1}x_l)\psi_n(m_lx_l)}{m_{l+1}\xi_n(m_lx_l)\psi_n'(m_lx_l) - m_{l+1}\xi_n'(m_lx_l)\psi_n(m_lx_l)}. \tag{28}$$

$$q^{mn}_{\mu\nu,l,12} = A^{mn}_{\mu\nu,l} \frac{m_{l+1}\psi_n(m_{l+1}x_l)\psi_n'(m_lx_l) - m_l\psi_n'(m_{l+1}x_l)\psi_n(m_lx_l)}{m_{l+1}\xi_n(m_lx_l)\psi_n'(m_lx_l) - m_{l+1}\xi_n'(m_lx_l)\psi_n(m_lx_l)}, \tag{29}$$

$$q^{mn}_{\mu\nu,l,13} = B^{mn}_{\mu\nu,l} \frac{m_{l+1}\xi_n(m_{l+1}x_l)\psi_n'(m_lx_l) - m_l\xi_n'(m_{l+1}x_l)\psi_n(m_lx_l)}{m_{l+1}\xi_n(m_lx_l)\psi_n'(m_lx_l) - m_{l+1}\xi_n'(m_lx_l)\psi_n(m_lx_l)}, \tag{30}$$

$$q^{mn}_{\mu\nu,l,14} = B^{mn}_{\mu\nu,l} \frac{m_{l+1}\psi_n(m_{l+1}x_l)\psi_n'(m_lx_l) - m_l\psi_n'(m_{l+1}x_l)\psi_n(m_lx_l)}{m_{l+1}\xi_n(m_lx_l)\psi_n'(m_lx_l) - m_{l+1}\xi_n'(m_lx_l)\psi_n(m_lx_l)}, \tag{31}$$

$$q^{mn}_{\mu\nu,l,21} = A^{mn}_{\mu\nu,l} \frac{m_l\xi_n'(m_{l+1}x_l)\xi_n(m_lx_l) - m_{l+1}\xi_n(m_{l+1}x_l)\xi_n'(m_lx_l)}{m_{l+1}\xi_n(m_lx_l)\psi_n'(m_lx_l) - m_{l+1}\xi_n'(m_lx_l)\psi_n(m_lx_l)}, \tag{32}$$

$$q^{mn}_{\mu\nu,l,22} = A^{mn}_{\mu\nu,l} \frac{m_l\psi_n'(m_{l+1}x_l)\xi_n(m_lx_l) - m_{l+1}\psi_n(m_{l+1}x_l)\xi_n'(m_lx_l)}{m_{l+1}\xi_n(m_lx_l)\psi_n'(m_lx_l) - m_{l+1}\xi_n'(m_lx_l)\psi_n(m_lx_l)}, \tag{33}$$

$$q^{mn}_{\mu\nu,l,23} = B^{mn}_{\mu\nu,l} \frac{m_l\xi_n'(m_{l+1}x_l)\xi_n(m_lx_l) - m_{l+1}\xi_n(m_{l+1}x_l)\xi_n'(m_lx_l)}{m_{l+1}\xi_n(m_lx_l)\psi_n'(m_lx_l) - m_{l+1}\xi_n'(m_lx_l)\psi_n(m_lx_l)}, \tag{34}$$

$$q^{mn}_{\mu\nu,l,24} = B^{mn}_{\mu\nu,l} \frac{m_l\psi_n'(m_{l+1}x_l)\xi_n(m_lx_l) - m_{l+1}\psi_n(m_{l+1}x_l)\xi_n'(m_lx_l)}{m_{l+1}\xi_n(m_lx_l)\psi_n'(m_lx_l) - m_{l+1}\xi_n'(m_lx_l)\psi_n(m_lx_l)}, \tag{35}$$

$$q^{mn}_{\mu\nu,l,31} = B^{mn}_{\mu\nu,l} \frac{m_{l+1}\xi_n'(m_{l+1}x_l)\psi_n(m_lx_l) - m_l\xi_n(m_{l+1}x_l)\psi_n'(m_lx_l)}{m_{l+1}\psi_n(m_lx_l)\xi_n'(m_lx_l) - m_{l+1}\psi_n'(m_lx_l)\xi_n(m_lx_l)}, \tag{36}$$

$$q^{mn}_{\mu\nu,l,32} = B^{mn}_{\mu\nu,l} \frac{m_{l+1}\psi_n'(m_{l+1}x_l)\psi_n(m_lx_l) - m_l\psi_n(m_{l+1}x_l)\psi_n'(m_lx_l)}{m_{l+1}\psi_n(m_lx_l)\xi_n'(m_lx_l) - m_{l+1}\psi_n'(m_lx_l)\xi_n(m_lx_l)}, \tag{37}$$

$$q^{mn}_{\mu\nu,l,33} = A^{mn}_{\mu\nu,l} \frac{m_{l+1}\xi_n'(m_{l+1}x_l)\psi_n(m_lx_l) - m_l\xi_n(m_{l+1}x_l)\psi_n'(m_lx_l)}{m_{l+1}\psi_n(m_lx_l)\xi_n'(m_lx_l) - m_{l+1}\psi_n'(m_lx_l)\xi_n(m_lx_l)}, \tag{38}$$

$$q^{mn}_{\mu\nu,l,34} = A^{mn}_{\mu\nu,l}\frac{m_{l+1}\psi'_n(m_{l+1}x_l)\psi_n(m_lx_l) - m_l\psi_n(m_{l+1}x_l)\psi'_n(m_lx_l)}{m_{l+1}\psi_n(m_lx_l)\xi'_n(m_lx_l) - m_{l+1}\psi'_n(m_lx_l)\xi_n(m_lx_l)}, \tag{39}$$

$$q^{mn}_{\mu\nu,l,41} = B^{mn}_{\mu\nu,l}\frac{m_l\xi_n(m_{l+1}x_l)\xi'_n(m_lx_l) - m_{l+1}\xi'_n(m_{l+1}x_l)\xi_n(m_lx_l)}{m_{l+1}\psi_n(m_lx_l)\xi'_n(m_lx_l) - m_{l+1}\psi'_n(m_lx_l)\xi_n(m_lx_l)}, \tag{40}$$

$$q^{mn}_{\mu\nu,l,42} = B^{mn}_{\mu\nu,l}\frac{m_l\psi_n(m_{l+1}x_l)\xi'_n(m_lx_l) - m_{l+1}\psi'_n(m_{l+1}x_l)\xi_n(m_lx_l)}{m_{l+1}\psi_n(m_lx_l)\xi'_n(m_lx_l) - m_{l+1}\psi'_n(m_lx_l)\xi_n(m_lx_l)}, \tag{41}$$

$$q^{mn}_{\mu\nu,l,43} = A^{mn}_{\mu\nu,l}\frac{m_l\xi_n(m_{l+1}x_l)\xi'_n(m_lx_l) - m_{l+1}\xi'_n(m_{l+1}x_l)\xi_n(m_lx_l)}{m_{l+1}\psi_n(m_lx_l)\xi'_n(m_lx_l) - m_{l+1}\psi'_n(m_lx_l)\xi_n(m_lx_l)}, \tag{42}$$

$$q^{mn}_{\mu\nu,l,44} = A^{mn}_{\mu\nu,l}\frac{m_l\psi_n(m_{l+1}x_l)\xi'_n(m_lx_l) - m_{l+1}\psi'_n(m_{l+1}x_l)\xi_n(m_lx_l)}{m_{l+1}\psi_n(m_lx_l)\xi'_n(m_lx_l) - m_{l+1}\psi'_n(m_lx_l)\xi_n(m_lx_l)}, \tag{43}$$

the solution of which yields the expansion coefficients in Eqs. (2)–(5).

The above boundary conditions must be satisfied for every interface and solved simultaneously for all the interfaces. For an L-layered core/shell particle, direct implementation of these conditions will lead to a linear equation of $4N(N+2)(L+1) \times 4N(N+2)(L+1)$ dimensions. As the number of shells (L) increases, the dimension of the linear system will grow drastically, resulting in an intensive computational task. However, a detailed analysis of the resulting matrix suggests that the matrix is largely block sparse, and one may take the advantage of this spareness of the matrix so that an efficient algorithm can be developed. Furthermore, if all these layers are concentered, then some of the block in the resulting matrix reduces to a diagonal matrix. Although a general-purpose sparse matrix may help to a certain extent in speeding up the computation, it will not be optimal as it cannot take full advantage of the block sparsity of the matrix for analytical expression. Our experience with multilayered core-shell structures further suggests that the block sparse matrix resulting from the multipole solution of the Maxwell equations may be further decomposed and simplified to obtain recursive relations, greatly simplifying the computations. This analysis of the matrix characteristics and electromagnetic fields associated with spherical coordinates has trusted us to develop a more efficient and robust computational algorithm for computing the coefficients of a core-shell structure of any layer. The algorithm solves each two-layered structure sequentially and progresses from the inner layer to the outer layer, the details of which are given below.

The above process in Eqs. (25)–(43) can be repeated for every layer in the multilayered particle, leading to the following crucial result that links the coefficients of the innermost core to the outmost shell,

$$\{ad\}^1 = [\mathrm{K}]\{ad\}^{L+1}, \tag{44}$$

with the global matrix [K] of dimensions $4N(N+2) \times 4N(N+2)$ related to $[\mathrm{Q}]_l$ as follows:

$$[\mathrm{K}] = \prod_{l=L}^{1}[\mathrm{Q}]_l. \tag{45}$$

Clearly, analytical expressions for $[\mathrm{K}]_l$, though very cumbersome, can be obtained once the geometry of the shell layers is defined.

For a plane wave incident on the particle, the fields of the incoming wave are expanded as

$$\mathbf{E}_{\mathrm{inc}} = \sum_{n=1}^{\infty}\sum_{m=-n}^{n} E_n\left(c_{mn}\mathbf{M}^{(1)}_{mn,L+1} + d_{mn}\mathbf{N}^{(1)}_{mn,L+1}\right), \tag{46}$$

$$\mathbf{H}_{\mathrm{inc}} = -\frac{im_{L+1}}{\omega\mu}\sum_{n=1}^{\infty}\sum_{m=-n}^{n} E_n\left(d_{mn}\mathbf{M}^{(1)}_{mn,L+1} + c_{mn}\mathbf{N}^{(1)}_{mn,L+1}\right), \tag{47}$$

with c_{mn} and d_{mn} are

$$c_{mn} = -E_0\frac{(2n+1)(n-m)!}{n(n+1)(n+m)!}i^n \times\left(\frac{d}{d\alpha}P^m_n(\cos\alpha)\sin\gamma - i\frac{m}{\sin\alpha}P^m_n(\cos\alpha)\cos\gamma\right), \tag{48}$$

$$d_{mn} = -E_0\frac{(2n+1)(n-m)!}{n(n+1)(n+m)!}i^n \times\left(\frac{m}{\sin\alpha}P^m_n(\cos\alpha)\sin\gamma - i\frac{d}{d\alpha}P^m_n(\cos\alpha)\cos\gamma\right). \tag{49}$$

According to Eqs. (2)–(5), $c^{L+1}_{mn} = c_{mn}$ and $d^{L+1}_{mn} = d_{mn}$, whereas, a^{L+1}_{mn} and b^{L+1}_{mn} are the scattering coefficients of the entire particle. For the innermost core, there is no outgoing field, which makes a^1_{mn} and b^1_{mn} 0. Rearrange the consequence of the coefficients from the order of $adbc$ to $abcd$, we get

$$\begin{bmatrix} 0 \\ 0 \\ c^1_{-N,N} \\ d^1_{-N,N} \\ \vdots \\ 0 \\ 0 \\ c^1_{mn} \\ d^{l+1}_{mn} \\ \vdots \end{bmatrix} = [\bar{\mathrm{K}}]\begin{bmatrix} a^{L+1}_{-N,N} \\ b^{L+1}_{-N,N} \\ c_{-N,N} \\ d_{-N,N} \\ \vdots \\ a^{L+1}_{\mu\nu} \\ b^{L+1}_{\mu\nu} \\ c_{\mu\nu} \\ d_{\mu\nu} \\ \vdots \end{bmatrix}, \tag{50}$$

with

$$[\bar{\mathrm{K}}]=\begin{bmatrix} [\bar{\mathrm{K}}]^{-N,N}_{-N,N} & [\bar{\mathrm{K}}]^{-N,N}_{-(N-1),N-1} & [\bar{\mathrm{K}}]^{-N,N}_{-(N-1),N} & \cdots & [\bar{\mathrm{K}}]^{-N,N}_{\mu\nu} & \cdots & [\bar{\mathrm{K}}]^{-N,N}_{NN} \\ [\bar{\mathrm{K}}]^{-(N-1),N-1}_{-N,N} & [\bar{\mathrm{K}}]^{-(N-1),N-1}_{-(N-1),N-1} & [\bar{\mathrm{K}}]^{-(N-1),N-1}_{-(N-1),N} & \cdots & [\bar{\mathrm{K}}]^{-(N-1),N-1}_{\mu\nu} & \cdots & [\bar{\mathrm{K}}]^{-(N-1),N-1}_{NN} \\ [\bar{\mathrm{K}}]^{-(N-1),N}_{-N,N} & [\bar{\mathrm{K}}]^{-(N-1),N}_{-(N-1),N-1} & [\bar{\mathrm{K}}]^{-(N-1),N}_{-(N-1),N} & \cdots & [\bar{\mathrm{K}}]^{-(N-1),N}_{\mu\nu} & \cdots & [\bar{\mathrm{K}}]^{-(N-1),N}_{NN} \\ \vdots & \vdots & \vdots & \ddots & \vdots & & \vdots \\ [\bar{\mathrm{K}}]^{mn}_{-N,N} & [\bar{\mathrm{K}}]^{mn}_{-(N-1),N-1} & [\bar{\mathrm{K}}]^{mn}_{-(N-1),N} & \cdots & [\bar{\mathrm{K}}]^{mn}_{\mu\nu} & \cdots & [\bar{\mathrm{K}}]^{mn}_{NN} \\ \vdots & \vdots & \vdots & & \vdots & \ddots & \vdots \\ [\bar{\mathrm{K}}]^{NN}_{-N,N} & [\bar{\mathrm{K}}]^{NN}_{-(N-1),N-1} & [\bar{\mathrm{K}}]^{NN}_{-(N-1),N} & \cdots & [\bar{\mathrm{K}}]^{NN}_{\mu\nu} & \cdots & [\bar{\mathrm{K}}]^{NN}_{NN} \end{bmatrix}. \tag{51}$$

Let us define

$$[\bar{\mathrm{K}}]^{mn}_{\mu\nu}=\begin{bmatrix} [\mathrm{A}]^{mn}_{\mu\nu} & [\mathrm{C}]^{mn}_{\mu\nu} \\ [\mathrm{B}]^{mn}_{\mu\nu} & [\mathrm{D}]^{mn}_{\mu\nu} \end{bmatrix}, \tag{52}$$

with

$$[\mathrm{A}]^{mn}_{\mu\nu}=\begin{bmatrix} \bar{k}^{mn}_{\mu\nu,11} & \bar{k}^{mn}_{\mu\nu,12} \\ \bar{k}^{mn}_{\mu\nu,21} & \bar{k}^{mn}_{\mu\nu,22} \end{bmatrix}, \quad [\mathrm{B}]^{mn}_{\mu\nu}=\begin{bmatrix} \bar{k}^{mn}_{\mu\nu,31} & \bar{k}^{mn}_{\mu\nu,32} \\ \bar{k}^{mn}_{\mu\nu,41} & \bar{k}^{mn}_{\mu\nu,42} \end{bmatrix}, \tag{53}$$

$$[\mathrm{C}]^{mn}_{\mu\nu}=\begin{bmatrix} \bar{k}^{mn}_{\mu\nu,13} & \bar{k}^{mn}_{\mu\nu,14} \\ \bar{k}^{mn}_{\mu\nu,23} & \bar{k}^{mn}_{\mu\nu,24} \end{bmatrix}, \quad [\mathrm{D}]^{mn}_{\mu\nu}=\begin{bmatrix} \bar{k}^{mn}_{\mu\nu,33} & \bar{k}^{mn}_{\mu\nu,34} \\ \bar{k}^{mn}_{\mu\nu,43} & \bar{k}^{mn}_{\mu\nu,44} \end{bmatrix}. \tag{54}$$

The global matrix $[\bar{\mathrm{K}}]$ becomes

$$[\bar{\mathrm{K}}]=\begin{bmatrix} [\mathrm{A}] & [\mathrm{C}] \\ [\mathrm{B}] & [\mathrm{D}] \end{bmatrix}. \tag{55}$$

Now, define vectors,

$$\{u\}^i=\begin{bmatrix} a^i_{-N,N} \\ b^i_{-N,N} \\ \vdots \\ a^i_{mn} \\ b^i_{mn} \\ \vdots \\ a^i_{N,N} \\ b^i_{N,N} \end{bmatrix}; \quad \{v\}^i=\begin{bmatrix} c^i_{-N,N} \\ d^i_{-N,N} \\ \vdots \\ c^i_{mn} \\ d^i_{mn} \\ \vdots \\ c^i_{N,N} \\ d^i_{N,N} \end{bmatrix}. \tag{56}$$

Equation (50) becomes

$$\begin{bmatrix} \{0\} \\ \{v\}^1 \end{bmatrix}=\begin{bmatrix} [\mathrm{A}] & [\mathrm{C}] \\ [\mathrm{B}] & [\mathrm{D}] \end{bmatrix}\begin{bmatrix} \{u\}^{L+1} \\ \{v\}^{L+1} \end{bmatrix}. \tag{57}$$

With elementary manipulations of Eq. (57), the Mie scattering coefficients of the particle are obtained

$$\{u\}^{L+1}=-[A]^{-1}_L[C]_L\{v\}^{L+1}. \tag{58}$$

With the scattering coefficients so determined, the scattering field is known, and integration of the Poynting vector of the scattering field over a spherical surface with its center at the outmost shell yields the scattering cross section of a multilayered eccentric particle,

$$C_{\mathrm{sca}}=\frac{4\pi}{k^2}\sum_{n=1}^{\infty}\sum_{m=-n}^{n}\frac{n(n+1)(n+m)!}{(2n+1)(n-m)!}\left(a^{L+1}_{mn}a^{*L+1}_{mn}+b^{L+1}_{mn}b^{*L+1}_{mn}\right)$$

$$=\frac{4\pi}{k^2}\sum_{n=1}^{\infty}\sum_{m=-n}^{n}\sum_{p=1}^{2}\frac{n(n+1)(n+m)!}{(2n+1)(n-m)!}\left(\{u\}^{L+1}_{mnp}\right), \tag{59}$$

with

$$\{u\}^{L+1}_{mnp}=\begin{cases} a^{L+1}_{mn} & p=1 \\ b^{L+1}_{mn} & p=2 \end{cases}. \tag{60}$$

Note that the presented algorithm involves L times of $4N(N+2)$ by the $4N(N+2)$-sized matrix multiplication operations rather than solving a $4N(N+2)(L+1)$ by $4N(N+2)(L+1)$ as the system. As the computational complexity of matrix multiplication and matrix inversion approach around $\mathrm{O}(n^{2.73})$ [49,50], the complexity of the algorithm proposed in this paper results in $\mathrm{O}(L(4N(N+2))^{2.73})$, whereas, the other well-known algorithms still require $\mathrm{O}((4N(N+2)(L+1))^{2.73})$.

For many scattering applications, only the scattering coefficients of the entire particle are required. For other applications, i.e., solar thermal engineering, the energy dissipated inside the particle is more important where the coefficients of inner layers are needed. With the presented progressive algorithm, the coefficients of a specific jth layer may be computed directly as

$$\begin{bmatrix} \{u\}^j \\ \{v\}^j \end{bmatrix}=[\mathrm{K}]_j\begin{bmatrix} \{u\}^{L+1} \\ \{v\}^{L+1} \end{bmatrix}, \tag{61}$$

with

$$[\mathrm{K}]_j=\prod_{l=L}^{j}[\mathrm{Q}]_l. \tag{62}$$

It is noteworthy that the coefficients of a such specific layer are obtained directly, rather than having to solve all the coefficients in between.

3. RESULTS AND DISCUSSIONS

Before exploring the optical responses of eccentric particles, we first show that the presented progressive methodology can be reduced to special cases, i.e., a solid sphere, a two-layered concentric shell, and an eccentric multilayered particle with all the inner layers displaced along an identical direction with certain assumptions.

A. Eccentric Particle with Enclosed Particles Displaced along a Line

This is a special case of an eccentric structure that has been studied in the literature with Ngo *et al*. perhaps being the first on the subject [48]. For this special case where all the displacements of inner layers are along the same direction, i.e., $\theta_{l,l+1}=0$, the associated Legendre polynomials become

$$P_p^{m-\mu}(\cos\theta_{l,l+1}) = P_p^{m-\mu}(1) = \delta_{m\mu}. \tag{63}$$

The addition coefficients $A_{mn}^{\mu\nu}$ and $B_{mn}^{\mu\nu}$ reduce to

$$A_{mn}^{\mu\nu}(l, l+1) = A_{mn}^{m\nu}(l, l+1)\delta_{m\mu},\ B_{mn}^{\mu\nu}(l, l+1) = B_{mn}^{m\nu}(l, l+1)\delta_{m\mu}. \tag{64}$$

As a result, all components with $\mu \neq m$ in Eq. (26) become [0]. $[Q]_l$ becomes a block-diagonal matrix with each component can be expressed as

$$[Q]_{m,l} = \begin{bmatrix} [Q]_{m,m,l}^{m,m} & [Q]_{m,m+1,l}^{m,m} & \cdots & [Q]_{m,\nu,l}^{m,m} & \cdots & [Q]_{m,N,l}^{m,m} \\ [Q]_{m,m,l}^{m,m+1} & [Q]_{m,m+1,l}^{m,m+1} & \cdots & [Q]_{m,\nu,l}^{m,m+1} & \cdots & [Q]_{m,N,l}^{m,m+1} \\ \vdots & \vdots & \ddots & \vdots & & \vdots \\ [Q]_{m,m,l}^{m,n} & [Q]_{m,m+1,l}^{m,n} & \cdots & [Q]_{m,\nu,l}^{m,n} & \cdots & [Q]_{m,N,l}^{m,n} \\ \vdots & \vdots & & \vdots & \ddots & \vdots \\ [Q]_{m,m,l}^{m,N} & [Q]_{m,m+1,l}^{m,N} & \cdots & [Q]_{m,\nu,l}^{m,N} & \cdots & [Q]_{NN,l}^{NN} \end{bmatrix}. \tag{65}$$

To show the above expressions for the scattering coefficients are compatible with reported works [48], the following mathematical manipulation is needed. With the above simplifications, Eq. (44) takes the form

$$\begin{aligned} \{ad\}_m^1 &= [\mathrm{K}]_m\{ad\}_m^3 \\ &= \prod_{l=2}^{1}[Q]_{m,l}\{ad\}_m^3 \\ &= [Q]_{m,2}[Q]_{m,1}\{ad\}_m^3. \end{aligned} \tag{66}$$

The above is equivalent to the work of Ngo *et al*. [48] with the following manipulations. Substitute Eqs. (6)–(9) and (29)–(32) into Eqs. (13) and (16) in the work of Ngo *et al*. [48], coefficients e_{nm}, f_{nm}, g_{nm}, h_{nm}, r_{nm}, s_{nm}, t_{nm}, and u_{nm} are then eliminated, leading to the same system of equations as Eq. (66) above. It is noteworthy that the coefficients a_{nm}, b_{nm}, c_{nm}, d_{nm}, p_{nm}, and q_{nm} in the work of Ngo *et al*. [48], are denoted as c_{mn}^3, d_{mn}^3, b_{mn}^3, a_{mn}^3, c_{mn}^1, and d_{mn}^1 in this paper, respectively. It is further noted that explicit expressions of the scattering coefficients of the eccentric particle could be obtained by following the same procedures through Eqs. (50)–(58) above; that is, the scattering cross section of the entire particle can be directly compared by substituting Eq. (58) into Eq. (59), instead of solving system equations.

B. Two-Layered Concentric Shell

It is shown that a concentric shell is basically a special case of the general algorithm presented here. For the case of a two-layered concentric shell, all the displacements of inner layers are 0, or all the inner spheres are centered at the same location. Physically, this means only certain modes are excited, and mathematically it means that the vector translation coefficients have special structures, namely,

$$A_{mn}^{\mu\nu}(l, l+1) = \delta_{m\mu}\delta_{n\nu}, \quad B_{mn}^{\mu\nu}(l, l+1) = 0. \tag{67}$$

This results in all components with $\nu \neq n$ in Eq. (65) being [0]. All the diagonal blocks in Eq. (65) now are independent of each other, which simplifies the linear system further into

$$\{ad\}_{mn}^l = [Q]_{mn,l}\{ad\}_{mn}^{l+1}, \tag{68}$$

with

$$\begin{aligned} [Q]_{mn,l} &= \begin{bmatrix} [Q]_{n,l,\mathrm{upper}} & [0] \\ [0] & [Q]_{n,l,\mathrm{lower}} \end{bmatrix} \\ &= \begin{bmatrix} q_{\mu\nu,l,11}^{mn} & q_{\mu\nu,l,12}^{mn} & 0 & 0 \\ q_{\mu\nu,l,21}^{mn} & q_{\mu\nu,l,22}^{mn} & 0 & 0 \\ 0 & 0 & q_{\mu\nu,l,33}^{mn} & q_{\mu\nu,l,34}^{mn} \\ 0 & 0 & q_{\mu\nu,l,43}^{mn} & q_{\mu\nu,l,44}^{mn} \end{bmatrix}. \end{aligned} \tag{69}$$

By setting $L = 2$ and substituting Eqs. (68) and (69) into Eq. (44), the scattering coefficients a_{mn}^3 and b_{mn}^3 can be calculated, yielding the same as reported in Ref. [21].

C. Solid Sphere

For the light-scattering problem of a solid sphere, Eq. (44) is further simplified with $L = 1$,

$$\{ad\}_{mn}^1 = [Q]_{mn,1}\{ad\}_{mn}^2, \tag{70}$$

expressions of coefficients a_{mn}^2 and b_{mn}^2 are obtained with the result,

$$a_{mn}^2 = -d_{mn}^2 \frac{\psi_n(x_l)\psi_n'(m_l x_l) - m_l\psi_n'(x_l)\psi_n(m_l x_l)}{\xi_n(x_l)\psi_n'(m_l x_l) - m_l\xi_n'(x_l)\psi_n(m_l x_l)}, \tag{71}$$

$$b_{mn}^2 = -c_{mn}^2 \frac{\psi_n'(x_l)\psi_n(m_l x_l) - m_l\psi_n(x_l)\psi_n'(m_l x_l)}{\xi_n'(x_l)\psi_n(m_l x_l) - m_l\xi_n(x_l)\psi_n'(m_l x_l)}. \tag{72}$$

For the case of light scattered by a plane wave, the incident wave expansion coefficients take the form of

$$c_{1n}^2 = -0.5i = d_{1n}^2, \quad c_{-1n}^2 = -0.5n(n+1)i = -d_{-1n}^2. \tag{73}$$

Furthermore, with the relations,

$$a_{1n}^2 = 0.5ia_n, \quad b_{1n}^2 = 0.5ib_n, \tag{74}$$

the Mie coefficients a_n and b_n, which are more frequently cited in the literature, are obtained below,

$$a_n = \frac{\psi_n(x_l)\psi_n'(m_l x_l) - m_l\psi_n'(x_l)\psi_n(m_l x_l)}{\xi_n(x_l)\psi_n'(m_l x_l) - m_l\xi_n'(x_l)\psi_n(m_l x_l)}, \tag{75}$$

$$b_n = \frac{\psi_n'(x_l)\psi_n(m_l x_l) - m_l\psi_n(x_l)\psi_n'(m_l x_l)}{\xi_n'(x_l)\psi_n(m_l x_l) - m_l\xi_n(x_l)\psi_n'(m_l x_l)}. \tag{76}$$

Once again, they are the same as reported in Ref. [25].

D. Numerical Results

This section presents a selection of some numerical results computed by the general progressive algorithm discussed above for different configurations. For the results presented in the following section, the incident wave is assumed to travel in the z direction with a linear polarization with **E** in the x direction.

Figure 2 plots the scattering efficiency of a void/SiO_2/Si three-layered rattling nanoshell. The inner void core has a radius

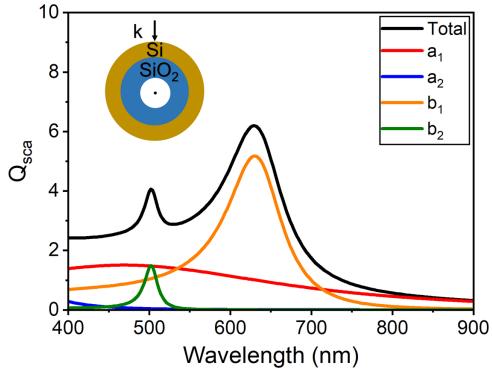

Fig. 2. Scattering efficiency with its electric and magnetic mode contributions (denoted as total, $a1$, $a2$, $b1$, and $b2$, respectively, as is the case throughout the paper) of a 40 nm/80 nm/100 nm void/SiO2/Si three-layered rattling concentric nanoshell.

of 40 nm, whereas, the thicknesses of the middle silica layer and the outmost silicon shell are 40 nm and 20 nm, respectively. The electric and magnetic mode components are denoted as a_n and b_n. The dipoles and quadrupoles correspond to 1 and 2 of n values, respectively, whereas, the scattering components of higher modes are negligible in this wavelength range. The results show that the dominating mode component is the magnetic dipole with its peak located around 640 nm, which originated from the circulation displacement with applied magnetic fields. The electric dipole, induced by the applied electric fields, is relatively insignificant since the void impedes the continuation of the displacement oscillation across the center of the particle. Therefore, a distinct magnetic mode is achieved in a relatively wide wavelength range without significant influences from other modes. It is not achievable in the case of a solid Si nanoparticle, where the magnetic dipole always partially overlaps with the electric dipole. Such separated response properties may be favorable for optical signal processing applications. The results computed using the general progressive algorithm for this concentric case are the same as those obtained by other methods.

Having studied the scattering characteristics of the concentric particle, we further explore the optical responses of eccentric particles. Figure 3 shows the scattering efficiency of a three-layered eccentric nanoshell. The radii and material compositions of the three layers are identical to that in Fig. 2,

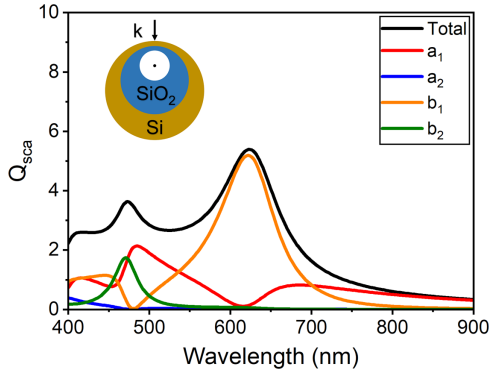

Fig. 3. Scattering efficiency with its electric and magnetic mode contributions of a 40 nm/80 nm/100 nm void/SiO_2/Si three-layered rattling eccentric nanoshell. The silica shell and the void core are displaced 18 nm against the wave propagation direction, respectively.

whereas, the inner void core and SiO_2 shell are displaced 18 nm along the $-\mathbf{k}$ direction. Compared to the concentric case, the resonance of the magnetic dipole is not shifted much since such displacements do not destroy the axisymmetry. A sharp peak of the electric dipole is observed around 490 nm, which is different from the flat peak with lower magnitudes in the concentric case. For the concentric case as shown in Fig. 2, the thickness (perpendicular to the wave propagation direction) of the particle varies gradually along the incidence wave; that is, the oscillating distances that form the electric dipole distribute evenly in a wide range, which results in a relatively lower peak in a wide wavelength range. However, the displacements in the eccentric case change the thickness drastically along the incidence wave. That is, the void in the top portion nearly impedes any oscillation, whereas, the bottom dielectric part has a relatively uniform thickness, yielding a concentrated resonance peak. In other words, simple displacements of the inner shell layers may adjust the electric dipole resonance, whereas, that of the magnetic dipole keeps the same. Such tunability is beneficial in assisting the design of multilayered particles to possess directional scattering features.

As studied the scattering of the eccentric particle with axisymmetry, we investigate the more general case that the displacements of the inner shells do not form a line. Figure 4 displays the scattering efficiency of a three-layered eccentric nanoshell with identical radii and material compositions of the above cases. The silica shell is displaced 18 nm along the direction that forms a 30° angle with the incident wave. The void core is displaced 18 nm along the direction that forms a −30° angle with the displacement direction of the silica shell. Both displacements are on the $E-k$ plane. From the result, multiple peaks of both electric and magnetic dipoles are observed at distinct wavelengths. Compared to the concentric case, the magnetic dipole is split into two relatively lower peaks at 640 nm and 470 nm, respectively. The electric dipole is separated into three peaks at 640 nm, 480 nm, and 410 nm, respectively. Such disordered displacement results in more complex thickness variations in the particle, which yields multiple peaks at different wavelengths. Compared to the concentric case, the effective circular oscillation distance is reduced, which leads to a second

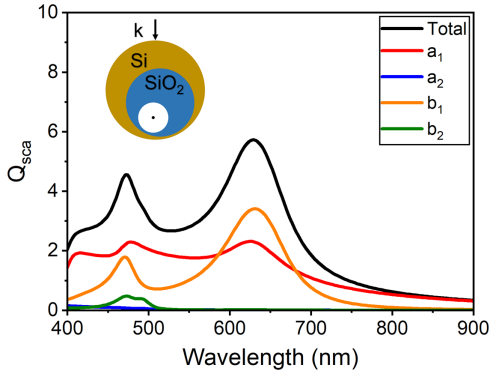

Fig. 4. Scattering efficiency with its electric and magnetic mode contributions of a 40 nm/80 nm/100 nm void/SiO2/Si three-layered rattling eccentric nanoshell. The silica shell is displaced 18 nm along the direction that forms a 30° angle with the incident wave, whereas, the void core is displaced 18 nm along the direction that forms a −30° angle with the displacement direction of the silica shell. Note that the angle is positive in the counterclockwise direction.

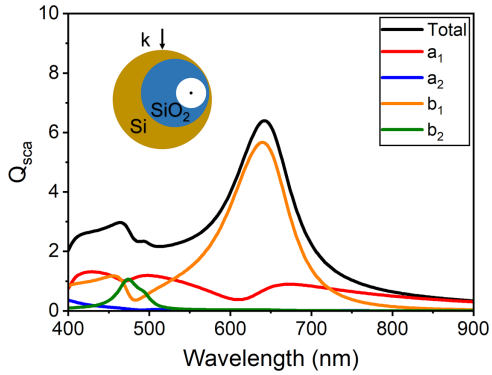

Fig. 5. Scattering efficiency with its electric and magnetic modes contributions of a 40 nm/80 nm/100 nm void/SiO2/Si three-layered rattling eccentric nanoshell. The silica shell is displaced 18 nm along the direction that forms a 120° angle with the incident wave, whereas, the void core is displaced 18 nm along the direction that forms a −30° angle with the displacement direction of the silica shell.

resonance peak at a higher frequency around 470 nm. It is also noted that the magnitudes of electric dipole resonances are relatively larger than those with the opposite displacements (the case in Fig. 3). The reason can be explained as follows. As the light penetrates the particle, the charges are more easily stretched along the electric-field direction due to the presence of a thick Si shell. As a consequence, the electric dipole resonance is more significant compared to the displacements opposite to the propagation direction where the light energy is dissipated before it reaches the bottom Si portion. Moreover, the magnitude of the peak at 640 nm is weakened due to the light attenuation effect at the top Si shell portion. In this case, it is shown that the peaks of both electric and magnetic dipoles can be tuned to the same frequency. With further fine adjustments, more optical behaviors, i.e., maximized forward scattering or enhanced transverse scattering could be achieved, which may be attractive for quantum dot emission and solar energy harvesting applications.

Figure 5 displays the scattering efficiency of the same eccentric nanoshell with different displacements of the inner shells. The silica shell is displaced 18 nm along the direction that forms a 120° angle with the incident wave. The void core is displaced 18 nm along the direction that forms a −30° angle with the displacement direction of the silica shell. The electric dipole mode has several lower peaks due to the thickness variation, whereas, the magnetic dipole still keeps a relatively large peak at 640 nm. Different from the case in Fig. 4, the light is not attenuated drastically on the top portion, which maintains the relatively large magnitude of the circular displacement current. It is worth noting that the magnitude of the magnetic dipole, in this case, is even larger than that in Fig. 3 where the SiO_2 shell and void core are displaced closer to the top. For the case in Fig. 5, the displacements of the inner cores are more along the horizontal direction. That is, different from the cases in Figs. 3 and 4, the thickness of layers along the electric-field direction is relatively uniform without the presence of a thick Si along the electric-field direction. Thus, the light is not attenuated significantly in the form of the electric dipole resonance, whereas, the magnetic dipole resonance is dominated.

As demonstrated in the above cases, the eccentricity of the inner shells provides extra freedom to adjust the resonance peaks of electric and magnetic modes, which may be useful to achieve broadband scattering properties.

4. CONCLUDING REMARKS

A general computational methodology had been presented for electromagnetic wave scattering by a multilayered eccentric particle. The computing algorithm was progressive in nature, starting with spherical vector wave translation, followed by matching the boundary conditions between adjacent layers progressively from the outmost to the innermost layer. One of the major advantages was that such a progressive approach significantly reduces the computation load for eccentric particle scattering by not having to solve an extremely large system of linear equations. Such a progressive procedure was also very useful in that explicit expressions of the scattering coefficients for the entire eccentric particle can be obtained. A salient feature of this algorithm was that it was applicable to complex eccentric core/shell structures with inner layers displaced along any direction. Moreover, the developed progressive algorithm was not only suitable for particles in the nanoscale, but also applicable for particles with any size parameters, although numerical examples shown were for nanosized particles. It was further shown that the presented methodology can be used to study practically any type of particle inclusions and the most widely studied cases, such as scattering by solid particles, concentric particles, and inclusions with centers displaced along a straight line were also special cases of the algorithm presented. Illustrative examples were also presented, demonstrating that the eccentric structure provided extra freedom in the design of multilayered nanoparticles to explore various optical phenomena.

Funding. Sunshine Energy Inc. (N028639).

Disclosures. The authors declare that there are no conflicts of interest related to this article.

Data availability. Data underlying the results presented in this paper are not publicly available at this time but may be obtained from the authors upon reasonable request.

REFERENCES

1. E. S. Arinze, B. Qiu, G. Nyirjesy, and S. M. Thon, "Plasmonic nanoparticle enhancement of solution-processed solar cells: practical limits and opportunities," ACS Photonics **3**, 158–173 (2016).
2. S. R. Mirnaziry, M. A. Shameli, and L. Yousefi, "Design and analysis of multi-layer silicon nanoparticle solar cells," Sci. Rep. **12**, 13259 (2022).
3. M. A. Shameli, S. R. Mirnaziry, and L. Yousefi, "Distributed silicon nanoparticles: an efficient light trapping platform toward ultrathin-film photovoltaics," Opt. Express **29**, 28037–28053 (2021).
4. T. Kawawaki, Y. Mori, K. Wakamatsu, S. Ozaki, M. Kawachi, S. Hossain, and Y. Negishi, "Controlled colloidal metal nanoparticles and nanoclusters: recent applications as cocatalysts for improving photocatalytic water-splitting activity," J. Mater. Chem. A **8**, 16081–16113 (2020).
5. M. Valenti, M. P. Jonsson, G. Biskos, A. Schmidt-Ott, and W. A. Smith, "Plasmonic nanoparticle-semiconductor composites for efficient solar water splitting," J. Mater. Chem. A **4**, 17891–17912 (2016).
6. Q. Zhang, D. T. Gangadharan, Y. Liu, Z. Xu, M. Chaker, and D. Ma, "Recent advancements in plasmon-enhanced visible light-driven water splitting," J. Mater. **3**, 33–50 (2017).

7. C. Collantes, V. González Pedro, M. J. Bañuls, and Á. Maquieira, "Monodispersed CsPb2Br5@SiO2 core-shell nanoparticles as luminescent labels for biosensing," ACS Appl. Nano Mater. **4**, 2011–2018 (2021).
8. Y. A. Hong and J. W. Ha, "Enhanced refractive index sensitivity of localized surface plasmon resonance inflection points in single hollow gold nanospheres with inner cavity," Sci. Rep. **12**, 1–9 (2022).
9. A. Loiseau, L. Zhang, D. Hu, M. Salmain, Y. Mazouzi, R. Flack, B. Liedberg, and S. Boujday, "Core-shell gold/silver nanoparticles for localized surface plasmon resonance-based naked-eye toxin biosensing," ACS Appl. Mater. Interfaces **11**, 46462–46471 (2019).
10. V. K. Gupta, S. Kumar, R. Kukreja, and N. Chander, "Experimental thermal performance investigation of a direct absorption solar collector using hybrid nanofluid of gold nanoparticles with natural extract of Azadirachta Indica leaves," Renew. Energy **202**, 1021–1031 (2023).
11. A. R. Mallah, M. N. M. Zubir, O. A. Alawi, S. N. Kazi, W. Ahmed, R. Sadri, and A. Kasaeian, "Experimental study on the effects of multi-resonance plasmonic nanoparticles for improving the solar collector efficiency," Renew. Energy **187**, 1204–1223 (2022).
12. Q. Wang, L. Yang, N. Zhao, G. Xu, J. Song, X. Jin, X. Li, and S. Liu, "A review of applications of plasmonic and conventional nanofluids in solar heat collection," Appl. Therm. Eng. **219**, 119476 (2023).
13. D. Ding, H. Wu, X. He, F. Yang, C. Gao, Y. Yin, and S. Ding, "A metal nanoparticle assembly with broadband absorption and suppressed thermal radiation for enhanced solar steam generation," J. Mater. Chem. A **9**, 11241–11247 (2021).
14. Y. Liu, J. Xiong, A. Li, R. Wang, L. Wang, and X. Qin, "Plasmonic silver nanoparticle-decorated electrospun nanofiber membrane for interfacial solar vapor generation," Text. Res. J. **91**, 2624–2634 (2021).
15. D. Wu, C. Zhao, Y. Xu, X. Zhang, L. Yang, Y. Zhang, Z. Gao, and Y.-Y. Song, "Modulating solar energy harvesting on TiO2 nanochannel membranes by plasmonic nanoparticle assembly for desalination of contaminated seawater," ACS Appl. Nano Mater. **3**, 10895–10904 (2020).
16. B. S. Luk'Yanchuk, N. V. Voshchinnikov, R. Paniagua-Domínguez, and A. I. Kuznetsov, "Optimum forward light scattering by spherical and spheroidal dielectric nanoparticles with high refractive index," ACS Photonics **2**, 993–999 (2015).
17. W. Liu, J. Zhang, B. Lei, H. Ma, W. Xie, and H. Hu, "Ultra-directional forward scattering by individual core-shell nanoparticles," Opt. Express **22**, 16178–16187 (2014).
18. H. K. Shamkhi, K. V. Baryshnikova, A. Sayanskiy, P. Kapitanova, P. D. Terekhov, P. Belov, A. Karabchevsky, A. B. Evlyukhin, Y. Kivshar, and A. S. Shalin, "Transverse scattering and generalized kerker effects in all-dielectric mie-resonant metaoptics," Phys. Rev. Lett. **122**, 193905 (2019).
19. H. Gong, W. Shao, X. Ma, and Z. Cui, "Absorption properties of a multilayer composite nanoparticle for solar thermal utilization," Opt. Laser Technol. **150**, 107914 (2022).
20. X. Yang, D. Bao, and B. Li, "Plasmon-mediated whispering-gallery-mode emission from quantum-dot-coated gold nanosphere," J. Phys. Chem. C **119**, 25476–25481 (2015).
21. X. Yang, Y. Li, and B. Li, "Silicon particle as a nanocavity for stable emission of quantum dots," ACS Photonics **4**, 2669–2675 (2017).
22. X. Yang, R. Xu, D. Bao, and B. Li, "Gold nanorod-enhanced light emission in quantum-dot-doped polymer nano fibers," ACS Appl. Mater. Interfaces **6**, 11846–11850 (2014).
23. X. Yang, R. Xu, L. Wen, Z. Lou, Q. Chen, and B. Li, "Light-induced thermal convection for collection and removal of carbon nanotubes," Fundam. Res. **2**, 59–65 (2022).
24. H. Yang, B. Q. Li, X. Jiang, W. Yu, and H. Liu, "Nano-fabrication of depth-varying amorphous silicon crescent shell array for light trapping," Nanotechnology **28**, 505301 (2017).
25. C. F. Bohren and D. R. Huffman, *Absorption and Scattering of Light by Small Particles* (Wiley, 1983).
26. A. L. Aden and M. Kerker, "Scattering of electromagnetic waves from two concentric spheres," J. Appl. Phys. **22**, 1242–1246 (1951).
27. R. Bhandari, "Scattering coefficients for a multilayered sphere: analytic expressions and algorithms," Appl. Opt. **24**, 1960–1967 (1985).
28. B. R. Johnson, "Light scattering by a multilayer sphere," Appl. Opt. **35**, 3286–3296 (1996).
29. Z. S. Wu, L. X. Guo, K. F. Ren, G. Gouesbet, and G. Gréhan, "Improved algorithm for electromagnetic scattering of plane waves and shaped beams by multilayered spheres," Appl. Opt. **36**, 5188–5198 (1997).
30. I. Gurwich, M. Kleiman, N. Shiloah, and A. Cohen, "Scattering of electromagnetic radiation by multilayered spheroidal particles: recursive procedure," Appl. Opt. **39**, 470–477 (2000).
31. Z. S. Wu and Y. P. Wang, "Electromagnetic scattering for multilayered sphere: recursive algorithms," Radio Sci. **26**, 1393–1401 (1991).
32. D. W. Mackowski and M. I. Mishchenko, "Calculation of the T matrix and the scattering matrix for ensembles of spheres," J. Opt. Soc. Am. A **13**, 2266–2278 (1996).
33. Y.-l. Xu, "Electromagnetic scattering by an aggregate of spheres," Appl. Opt. **34**, 4573–4588 (1995).
34. Y.-l. Xu and N. G. Khlebtsov, "Orientation-averaged radiative properties of an arbitrary configuration of scatterers," J. Quant. Spectrosc. Radiat. Transf. **79–80**, 1121–1137 (2003).
35. D. W. Mackowski, "Analysis of radiative scattering for multiple sphere configurations," Proc. R. Soc. London. A **433**, 599–614 (1991).
36. J. Sancho-Parramon, "Surface plasmon resonance broadening of metallic particles in the quasi-static approximation: a numerical study of size confinement and interparticle interaction effects," Nanotechnology **20**, 235706 (2009).
37. R.-L. Chern, X.-X. Liu, and C.-C. Chang, "Particle plasmons of metal nanospheres: application of multiple scattering approach," Phys. Rev. E **76**, 016609 (2007).
38. M. Sadrara and M. F. Miri, "Faraday rotation spectrum of magneto-optical nanoparticle aggregates," Phys. Rev. B **96**, 115436 (2017).
39. M. Sadrara and M. F. Miri, "Scattering of electromagnetic waves by an aggregate of gyromagnetic and dielectric spheres: magnetic tuning of Fano resonances," Phys. Rev. B **101**, 064426 (2020).
40. W. Liu, "Ultra-directional super-scattering of homogenous spherical particles with radial anisotropy," Opt. Express **23**, 14734–14743 (2015).
41. W. Yang, "Improved recursive algorithm for light scattering by a multilayered sphere," Appl. Opt. **42**, 1710–1720 (2003).
42. O. Peña and U. Pal, "Scattering of electromagnetic radiation by a multilayered sphere," Comput. Phys. Commun. **180**, 2348–2354 (2009).
43. O. R. Cruzan, "Translational addition theorems for spherical vector wave functions," Q. Appl. Math. **20**, 33–40 (1962).
44. S. Stein, "Addition theorems for spherical wave functions," Q. Appl. Math. **19**, 15–24 (1961).
45. C. Liu and B. Q. Li, "Computational multiscattering of spherical multilayered gold nanoshells," J. Phys. Chem. C **115**, 5323–5333 (2011).
46. A. Moroz, "A recursive transfer-matrix solution for a dipole radiating inside and outside a stratified sphere," Ann. Phys.-New York **315**, 352–418 (2005).
47. R. Li and B. Q. Li, "Efficient progressive algorithm for light scattering of a multilayered concentric nanoparticle," Appl. Opt. **61**, 10556–10566 (2022).
48. D. Ngo, G. Videen, and P. Chýlek, "A FORTRAN code for the scattering of EM waves by a sphere with a nonconcentric spherical inclusion," Comput. Phys. Commun. **99**, 94–112 (1996).
49. R. Duan, H. Wu, and R. Zhou, "Faster matrix multiplication via asymmetric hashing," arXiv, arXiv:2210.10173 (2022).
50. A. M. Davie and A. J. Stothers, "Improved bound for complexity of matrix multiplication," Proc. R. Soc. Edinburgh A Math. **143A**, 351–370 (2013).